Winter Precipitation Patterns in Arctic Alaska Determined from a Blowing-Snow Model and Snow-Depth Observations

GLEN E. LISTON

Department of Atmospheric Science, Colorado State University, Fort Collins, Colorado

MATTHEW STURM

U.S. Army Cold Regions Research and Engineering Laboratory—Alaska, Fort Wainwright, Alaska

(Manuscript received 8 October 2001, in final form 12 July 2002)

ABSTRACT

A blowing-snow model (SnowTran-3D) was combined with field measurements of end-of-winter snow depth and density to simulate solid (winter) precipitation, snow transport, and sublimation distributions over a 20 000-km^2 arctic Alaska domain. The domain included rolling uplands and a flat coastal plain. Simulations were produced for the winters of 1994/95, 1995/96, and 1996/97. The model, which accounts for spatial and temporal variations in blowing-snow sublimation, as well as saltation and turbulent-suspended transport, was driven with interpolated fields of observed temperature, humidity, and wind speed and direction. Model outputs include local (a few hundreds of meters) to regional (several tens of kilometers) distributions of winter snow-water-equivalent depths and blowing-snow sublimation losses, from which the regional winter precipitation distributions are computed. At regional scales, the end-of-winter snow depth is largely equal to the difference between winter precipitation and moisture loss due to sublimation. While letting SnowTran-3D simulate the blowing-snow sublimation fluxes, the precipitation fields were determined by forcing the regional variation in model-simulated snow depths to match measured values. Averaged over the entire domain and the three simulation years, the winter precipitation was 17.6 cm, with uplands values averaging 19.0 cm and coastal values averaging 15.3 cm. On average, 21% of the precipitation was returned to the atmosphere by blowing-snow sublimation, while in the windier coastal regions 34% of the winter precipitation sublimated.

1. Introduction

Throughout the arctic, much of the winter precipitation falls as a solid, influencing numerous components of the high-latitude hydrologic cycle. As the winter progresses, this precipitation accumulates on the ground, building a snow cover that affects atmospheric and soil temperatures by moderating conductive, sensible, and latent energy transfers between the atmosphere, snow cover, and ground (e.g., Hinzman et al. 1998; Nelson et al. 1998; Liston 1999). During snowmelt in the spring, the release of this precipitation also impacts snow–land–atmosphere energy exchanges (e.g., Liston 1995; Neumann and Marsh 1998), and soil-moisture conditions, runoff, and active layer characteristics (e.g., Kane et al. 1991; Everett et al. 1996; Hinzman et al. 1996; McNamara et al. 1997, 1998, 1999; Marsh 1999).

Unfortunately, accurate arctic solid-precipitation measurements have proven nearly impossible to achieve because this precipitation generally falls when it is windy, and precipitation gauges located in windy environments significantly underestimate solid-precipitation amounts (Larson and Peck 1974; Goodison et al. 1981; Benson 1982; Yang et al. 1998, 2000). Even the most advanced and complex shielded precipitation gauges, such as the World Meteorological Organization (WMO) Solid Precipitation Measurement Intercomparison Project's ''octagonal vertical Double Fence Intercomparison Reference'' (DFIR), are unable to measure the true precipitation (liquid or solid) and require corrections for wind speed (Yang et al. 1998). Additional complications include the generally sparse precipitation measurement network in remote arctic areas, and the unattended operation of many gauges in these areas. In combination, these inherent problems lead us to conclude that, even though quantifying solid-precipitation distributions across different landscapes is critical to understanding and modeling the earth's climate system, these precipitation distributions are virtually unknown. This ignorance of such a fundamental climate-system component is a serious impediment to many arctic hydrologic, atmospheric, and ecological research efforts,

Corresponding author address: Dr. Glen E. Liston, Department of Atmospheric Science, Colorado State University, Fort Collins, CO 80523-1371.
E-mail: liston@atmos.colostate.edu

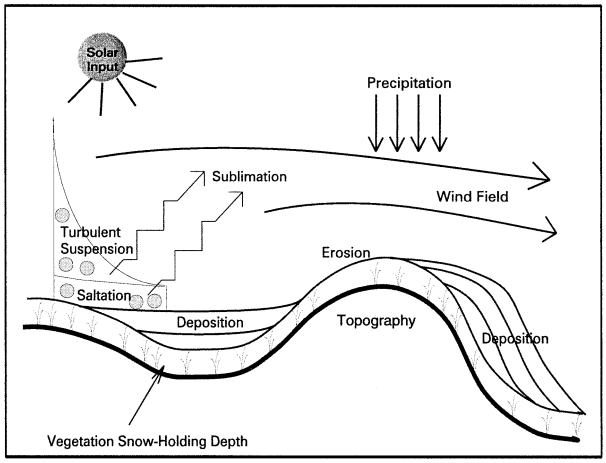

FIG. 1. Key features of the SnowTran-3D model (following Liston and Sturm 1998).

and there is a strong need to develop alternative methods to determine solid-precipitation distributions.

During a series of over-snow traverses in arctic Alaska between 1994 and 1997, we found that we could make detailed snow-water-equivalent depth measurements over 200-km-long observational transects (König and Sturm 1998; M. Sturm and G. E. Liston 2001, unpublished manuscript, hereafter SL; Taras et al. 2002). It was tantalizing to realize that if we could account for blowing-snow redistribution and sublimation, then these snow-depth measurements could be converted into a measure of the winter solid precipitation. This became possible with the development of a blowing-snow model (SnowTran-3D; Liston and Sturm 1998) that simulates snow-transport and sublimation processes (Fig. 1).

Arctic tundra snow covers are typically thin (<60 cm), and the frequent occurrence of blowing snow leads to significant snow redistribution. This redistributed snow erodes from higher-wind-speed areas, like ridge tops, and accumulates in lower-wind-speed areas, like the lees of ridges, topographic depressions, and taller vegetation (Benson and Sturm 1993; Pomeroy et al. 1993; Liston and Sturm 1998; SL; Sturm et al. 2001a,b; Liston et al. 2002). If wind-transported snow is not deposited in some kind of drift trap, and if the blowing-snow event lasts long enough and the air remains unsaturated, then the particles can eventually sublimate away. Tabler (1975) introduced the idea of particle transport distance: the distance an average-sized snow/ice grain can travel before it completely sublimates. For Wyoming, he found transport distances of approximately 3 km. By applying the same ideas to arctic Alaska, Benson (1982) calculated transport distances of 2–3 km for a region south of Barrow, Alaska. As a consequence of the vigorous wind transport, a significant portion (5%–50%) of the arctic snowcover is returned to the atmosphere by sublimation of the wind-borne snow particles (Benson 1982; Liston and Sturm 1998; Essery et al. 1999; Pomeroy and Essery 1999). In Canada, estimates of the amount of solid precipitation that sublimates range from 15% to 41% on the Canadian prairies (Pomeroy and Gray 1995), and from 20% to 47% in the Trail Valley Creek area of the western Canadian arctic (Pomeroy et al. 1997; Essery et. al. 1999). These high rates are achieved during blowing-snow events because of the relatively high particle surface-area–to–mass ratio and high particle ventilation rates (Schmidt 1972); they are much higher (as much as two orders of magnitude) than those found on a static snow surface under the same atmospheric conditions (Schmidt 1982). Blowing-snow sublimation rates are most strongly dependent upon air temperature, humidity deficit, wind speed, and particle size distribution (Schmidt 1972, 1982; Tabler 1975; Pomeroy and Gray 1995). As evidence of the importance of blowing-snow sublimation in arctic Alaska, we find that only when we include blowing-snow sublimation processes in our arctic Alaska simulations do we reproduce the observed snow distributions (Liston and Sturm 1998).

In what follows, we present a methodology to derive regional winter solid-precipitation distributions from a combination of SnowTran-3D model simulations and sparsely distributed snow-depth measurements. The methodology is applied over a 20 000-km^2 area of arctic Alaska. Because of blowing-snow redistribution and sublimation processes, the snow distribution within this domain varies on a local scale of a few hundreds of meters. It also varies on a regional scale of several tens of kilometers, in response to regional precipitation, air temperature, humidity, and wind speed and direction gradients.

Previous arctic, three-dimensional, full-winter, blowing-snow simulations have been performed by Liston and Sturm (1998) over a 6-km^2 Alaska domain; by Bruland et al. (2002) over 25- and 250-km^2 domains in Svalbard, Norway; by Hasholt et al. (2002) over a 256-km^2 eastern Greenland domain (all using SnowTran-3D); and by Essery et al. (1999) over a 168-km^2 Canadian domain, using a spatially distributed version of the Prairie Blowing Snow Model (PBSM; Pomeroy et al. 1993). Because of their relatively small domains, these previous studies did not address regional precipitation gradients.

2. Methods

a. Study domain

Winter precipitation and snowcover evolution were simulated from 1 September through 30 April for the years 1994/95, 1995/96, and 1996/97. In the following discussion, these simulation periods are referred to as 1995, 1996, and 1997, respectively. The spatial domain covers an 85 km $\times$ 230 km region in arctic Alaska that is bounded by the Brooks Range to the south and the Arctic Ocean to the north, and includes the Kuparuk River basin (Fig. 2). The southern and

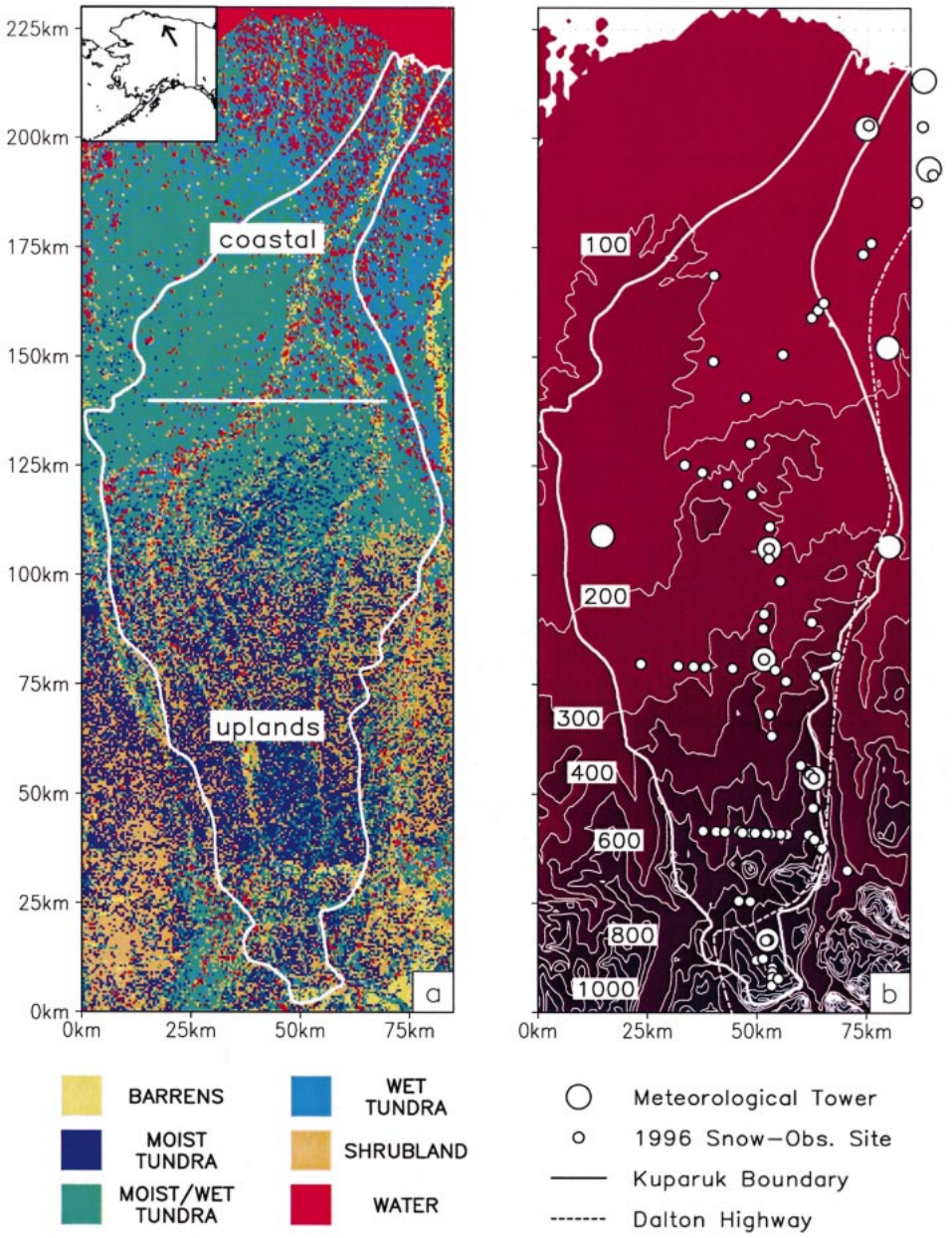

FIG. 2. Kuparuk basin simulation domain showing (a) vegetation and (b) topography (100-m contour interval). Also shown are the basin boundary, Dalton Highway, meteorological towers, and snow-data collection sites used in 1996. The inset figure identifies the general location of the Kuparuk basin within arctic Alaska, and (a) identifies the general coastal and uplands subregions. The domain coordinates can be converted to UTM by adding 354 km to the west–east origin (easting) and 7596 km to the south–north origin (northing) and converting to meters. (Data courtesy of D. A. Walker, Institute of Arctic Biology, University of Alaska, Fairbanks.)

northern boundaries of the domain are at approximately 68°28′ and 70°32′N latitude, respectively. Vegetation within this domain ranges from rocky barrens in some river bottoms, to low-growing tundra vegetation types, to taller shrub vegetation located in hillside water tracks and along streams and rivers (Fig. 2a). In the southern portion of the domain the topography is characterized by gently rolling ridges and valleys referred to as ''uplands,'' and the northern portion is generally flat and referred to as ''coastal'' (Fig. 2b); the uplands–coastal boundary occurs near the 100-m elevation contour (Fig. 2b) at a south–north position of roughly 140 km (Fig. 2a). During the ''winter'' months (September–April), air temperatures are usually below freezing and virtually all precipitation falls as a solid (Olsson et al. 2002).

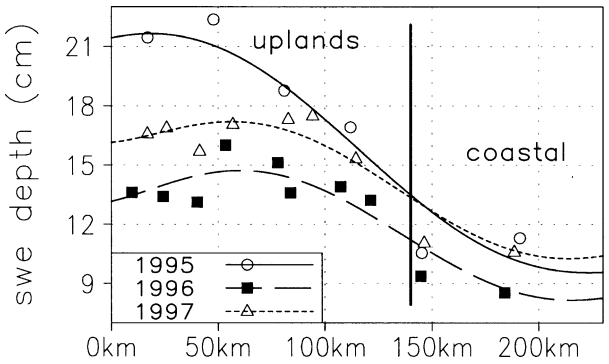

FIG. 3. South–north variation of observed Kuparuk basin end-of-winter snow-water-equivalent (swe) depths for 1995, 1996, and 1997 for ''intermediate'' areas only (see text). Shown are the sixth-order polynomial fits (lines) to the clustered measurements (markers). Also shown are the general coastal and uplands subregions. The abscissa values correspond to the ordinate values in Fig. 2.

b. Snow observations

In April of 1995, 1996, and 1997 we traversed from the headwaters of the Kuparuk basin to the arctic coast, making extensive snow-depth and density measurements. These measurements were made within a few weeks of the snowmelt period and are considered to closely represent end-of-winter values. In 1996, we made snow measurements at the 71 sites identified in Fig. 2b; a slightly different number of sites and locations were occupied in 1995 and 1997. At each site, 201 depth measurements (König and Sturm 1998; SL; Taras et al. 2002) were made on hundred-meter lines (approximately 14 000 snow-depth measurements on each traverse). By making numerous measurements along the hundred-meter lines, each measurement site provided a measure of the local snow distribution instead of just a ''point'' value. In addition, at these sites 10 snow cores were obtained and used to compute the snow-water-equivalent depth, and snow density was measured layer by layer in 5 snow pits. Snow-pit and -core density measurements agreed to within 1.5%. Based on these data, a relationship between snow depth and snow density was developed that allowed us to convert from one to the other (see SL). Coastal densities were slightly higher than uplands densities, but the differences were too small to warrant using spatially varying snow densities in the model simulations. Thus, we convert between snow depth and snow-water-equivalent depth using winter-average bulk density values of 295, 255, and 270 kg m^{-3} for 1995, 1996, and 1997, respectively.

To determine the regional (south–north) snow-depth trends for each traverse, the 201 snow-depth measurements from each site were averaged, and the sites were classified as exposed areas (e.g., ridges; 11 in 1996), sheltered areas (e.g., valleys and creeks; 12 in 1996), or intermediate areas (e.g., flat or gentle slopes; 48 in 1996) (see Taras et al. 2002). Because of the extreme local snow-depth variability found in the exposed and sheltered areas, only the intermediate data were used to define the regional trends. The intermediate data were grouped into discrete bands and the mean snow depth was calculated for each band. For example, there were 10 east–west bands in 1996, each spanning about 20 km from south to north. These data are plotted in Fig. 3, along with a sixth-order polynomial fit to those data. The polynomial coefficients are listed in Table 1. The trends are similar for the three years except for two high values from the southern uplands recorded in 1995.

TABLE 1. Coefficients used to define the sixth-order polynomials describing the observed snow-water-equivalent depth distributions (cm) (Fig. 3), in the form $\zeta^*(y) = c_1 + c_2y + c_3y^2 + c_4y^3 + c_5y^4 + c_6y^5$, where $0 \le y \le 230$ km.

	1995	1996	1997
c_1	21.428	13.158	16.145
c_2	2.060×10^{-2}	2.608×10^{-2}	1.030×10^{-2}
c_3	-4.211×10^{-4}	6.520×10^{-4}	8.401×10^{-4}
c_4	-5.641×10^{-6}	-1.486×10^{-5}	-1.640×10^{-5}
c_5	4.461×10^{-8}	7.378×10^{-8}	8.004×10^{-8}
c_6	-7.850×10^{-11}	-1.104×10^{-10}	-1.196×10^{-10}

SL showed that there are two distinctly different snow regimes across the Kuparuk basin, uplands and coastal, and represented these by independent uplands and coastal regression curves (leading to a discontinuity at the uplands–coastal boundary). However, the depth contrast across the discontinuity is not large. Therefore, to simplify the modeling, in this paper we represent the south–north snow-depth variations in the basin as continuous functions.

c. Model description

SnowTran-3D is a three-dimensional model that simulates snow-depth evolution over topographically variable terrain (Fig. 1). The model was originally developed and tested in an arctic tundra landscape (Liston and Sturm 1998) but is generally applicable to other treeless areas characterized by sufficiently strong winds, below-freezing temperatures, and solid precipitation (Greene et al. 1999; Liston et al. 2000; Prasad et al. 2001; Hiemstra et al. 2002). SnowTran-3D's primary components are 1) the wind-flow forcing field, 2) the wind shear stress on the surface, 3) the transport of snow by saltation, 4) the transport of snow by turbulent suspension, 5) the sublimation of saltating and suspended snow, and 6) the accumulation and erosion of snow at the snow surface. The required model inputs are 1) spatially distributed temporally varying fields of precipitation, wind speed and direction, air temperature, and humidity, obtained from meteorological stations located within the simulation domain and/or an atmospheric model; and 2) spatially distributed fields of topography and vegetation type. Within the model, each grid cell is assigned a single vegetation type, and each vegetation type is assigned a canopy height that defines the vegetation snow-holding depth. The snow depth must ex-

ceed the vegetation snow-holding depth before snow becomes available for wind transport (i.e., snow captured within the vegetation canopy by either precipitation or blowing-snow deposition cannot be removed by the wind). Because of these important snow–vegetation interactions (McFadden et al. 2001; Sturm et al. 2001b; Liston et al. 2002), SnowTran-3D simulates the snow-depth evolution and then uses the snow density to convert to the more hydrologically significant snow-water equivalent.

The foundation of SnowTran-3D is a mass-balance equation that describes the temporal variation of snow depth at each point within the simulation domain (Liston and Sturm 1998). Deposition and erosion, which lead to changes in snow depth at these points, are the result of 1) changes in horizontal mass-transport rates of saltation, Q_{salt} (kg m^{-1} s^{-1}); 2) changes in horizontal mass-transport rates of turbulent-suspended snow, Q_{turb} (kg m^{-1} s^{-1}); 3) sublimation of transported snow particles, Q_v (kg m^{-2} s^{-1}); and 4) the water-equivalent precipitation rate, P (m s^{-1}). Combined, the time rate of change of snow depth, ζ (m), is

$$\frac{d\zeta}{dt} = \frac{1}{\rho_s}\left[\rho_w P - \left(\frac{dQ_{\text{salt}}}{dx} + \frac{dQ_{\text{turb}}}{dx} + \frac{dQ_{\text{salt}}}{dy} + \frac{dQ_{\text{turb}}}{dy}\right) + Q_v\right], \tag{1}$$

where t (s) is time; x (m) and y (m) are the horizontal coordinates in the west–east and south–north directions, respectively; and ζ_s and ζ_w (kg m^{-3}) are the snow and water density, respectively. At each time step, Eq. (1) is solved for each individual grid cell within the domain and is coupled to the neighboring cells through the spatial derivatives (d/dx, d/dy). In this formulation, we have assumed that sublimation from a static snow surface (no blowing snow) is negligible compared to the blowing-snow sublimation fluxes; the latter can be more than 100 times larger than the former.

The results of this paper rely heavily on the formulation of the sublimation term, Q_v, in Eq. (1). Our sublimation model follows that of Schmidt (1972, 1991), Pomeroy et al. (1993), and Pomeroy and Gray (1995), where the sublimation rate of transported snow, per unit area of snow cover, Q_v, is given by

$$Q_v(x^*) = \int_0^{z_t} \Psi(x^*, z)\varphi(x^*, z)\, dz, \tag{2}$$

where x^* (m) is the horizontal coordinate (in a reference frame defined by the wind-flow direction); z (m) is the height coordinate; Ψ (s^{-1}) is the sublimation-loss-rate coefficient; φ (kg m^{-3}) is the mass concentration of the snow-particulate ''cloud''; and the integration limits are from the snow surface through the saltating layer to the top of the turbulent-transport layer (at $z = z_t$).

The sublimation-loss-rate coefficient, Ψ, describes the rate of particle mass loss as a function of height within the blowing and drifting snow profile, and is a function of 1) temperature-dependent humidity gradients between the snow particle and the atmosphere, 2) conductive and advective energy and moisture transfer mechanisms, 3) particle size, and 4) solar radiation intercepted by the particle. In addition, we assume that (i) the mean particle size decays exponentially with height; (ii) the relative humidity follows a logarithmic distribution, decreasing with height; (iii) the air temperature in the snow-transport layer is well mixed and constant with height; (iv) the variables defined within the saltation layer are constant with height, and those in the turbulent-suspension layer vary with height; and (v) the solar radiation absorbed by snow particles is a function of the solar elevation angle (latitude, time of day, day of year) and fractional cloud cover. Complete formulation details for each term in Eqs. (1) and (2) can be found in Liston and Sturm (1998).

TABLE 2. Vegetation snow-holding depth (SHD) used in the model simulations, in units of cm snow depth. Also shown is the areal fraction covered by each vegetation type.

	Vegetation SHD (cm)	Fraction of domain covered (%)
Barrens	5	3
Moist tundra	10	20
Moist/wet tundra	20	40
Wet tundra	8	9
Shrubland	40	18
Water	0	10

The simulations used a 100 m × 100 m horizontal grid spacing and a 1-day time step. The grid spacing and time step were chosen to be compatible with available datasets and to minimize computational expense over this relatively large domain. In areas where the observed topographic variability is not described by the 100-m grid increment, like sharp ridges and river-cut banks, the simulated snow distribution will be smoother than in the natural system. In a similar way, snow-transport events that are shorter than the 1-day time step will not be well represented by the model; for simulations spanning the entire snow season, we have not found this to be a significant problem, largely because wind events strong enough to transport snow usually last longer than 1 day.

The snow-holding depth for, and fraction of the domain covered by, each vegetation type are given in Table 2. Although it depends on many factors, we have found that the snow-holding depth for arctic vegetation generally lies between the average and the maximum vegetation height, with 80% of the maximum vegetation height usually yielding an appropriate vegetation snow-holding depth; to determine these values we used vegetation data from Bliss and Matveyeva (1992). The snow density for each of the years was defined based on our observations discussed in the previous section. All other SnowTran-3D user-defined constants are the same as those used by Liston and Sturm (1998). Because of the significant fraction of lakes in the simulation domain

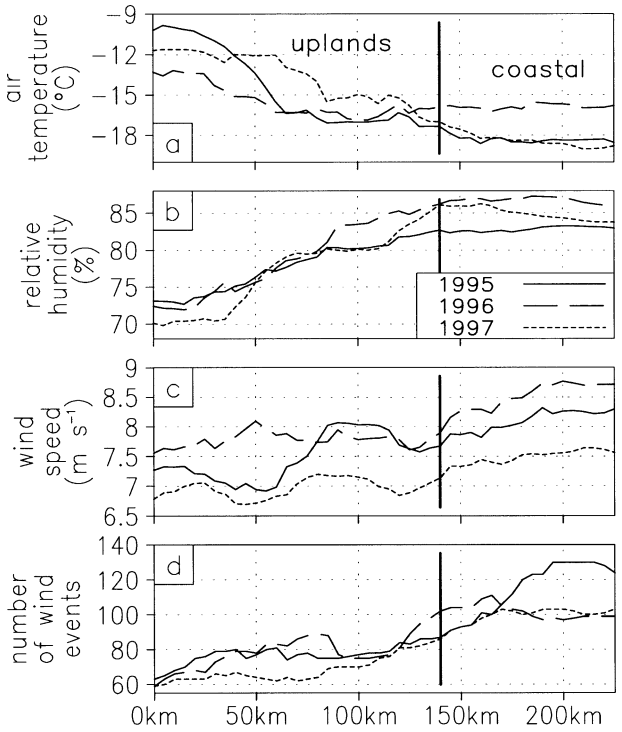

FIG. 4. Winter-averaged, south–north variation in meteorological forcing used in model simulations for 1995, 1996, and 1997, for daily averaged wind speeds greater than 5 m s^{-1}: (a) air temperature, (b) relative humidity, and (c) wind speed. Also shown are (d) the number of events (days) when the wind speed was greater than 5 m s^{-1}. The abscissa values correspond to the ordinate values in Fig. 2, and the general coastal and uplands subregions are indicated. (Data, in part, courtesy of Douglas L. Kane and Larry D. Hinzman, Water and Environmental Research Center, University of Alaska, Fairbanks.)

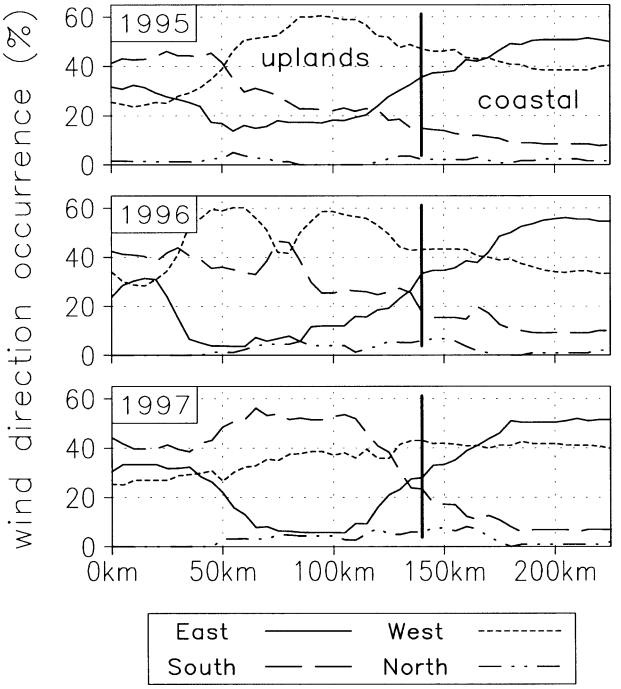

FIG. 5. South–north variation of Kuparuk basin wind directions for 1995, 1996, and 1997. Shown is the fraction of winter daily averaged wind speeds greater than 5 m s^{-1}, for a window covering $\pm 45°$ of each cardinal direction. Also shown are the general coastal and uplands subregions. The abscissa values correspond to the ordinate values in Fig. 2.

(Fig. 2a), any model grid cell classified as inland water was not allowed to accumulate snow, by precipitation or blowing-snow mechanisms, until after its surface was frozen; any such moisture fell into the unfrozen lake. Based on arctic Alaska lake ice model simulations (Liston and Hall 1995; Jeffries et al. 1996), a 12 September freeze-up date was defined for each of the simulation years. Because of their lack of roughness elements to capture and hold snow, frozen inland-water grid cells (Fig. 2a) are assumed to have a vegetation snow-holding depth of 0 cm (Table 2).

d. Atmospheric forcing

SnowTran-3D was driven with air temperature, humidity, and wind speed and direction data from two of our meteorological stations, and eight of those run by the Water and Environmental Research Center, University of Alaska, Fairbanks (Fig. 2b). These meteorological stations do not measure winter precipitation; our method to determine the precipitation is discussed in the following section. There are three Natural Resources Conservation Service gauges within the simulation domain that measure winter precipitation; data from these gauges will be compared with our model outputs in the results section.

The meteorological data were interpolated to the spatially and temporally continuous form required by SnowTran-3D (values at each grid point and for every model time step) using the following procedures: since not all of the towers were the same height, we assumed a logarithmic wind profile and vertically interpolated the wind speed data to a common 10-m level using a roughness length of 0.001 m under the assumption of a sastrugi-covered snow surface. Because the station distribution was not sufficient to capture west–east gradients throughout the domain (there is only one station in the western portion of the domain; Fig. 2b), we used the datasets to define only the south–north meteorological variations. Our field measurements along two east–west cross lines (Fig. 2) suggest that the regional east–west gradients are small; this assumption is further supported by the relatively narrow width of the domain. For each model time step the available station data were gridded to the model grid using an inverse-square-weighting interpolation procedure. The resulting south–north variations in atmospheric forcings are summarized in Figs. 4 and 5. As part of the model simulations, the south–north wind speed distributions were modified using the empirical wind–topography relationship described in Liston and Sturm (1998), where the wind speeds are locally increased on ridges and windward

slopes, and locally decreased in topographic depressions and on lee slopes. The values presented in Figs. 4 and 5 are winter averages that include only those days when the wind speeds were greater than 5 m s^{-1}. This 5 m s^{-1} value was chosen because it has been observed to be the lower bound for blowing snow occurrence within arctic Alaska (Sturm et al. 2001a); values below this threshold were not included so that Figs. 4 and 5 would more closely display atmospheric conditions found during snow transport when redistribution and sublimation are important.

Figure 4 shows that during all three years the air temperature decreased from the uplands to the uplands–coastal boundary and was fairly constant from there to the coast. The relative humidity increased from the uplands to the uplands–coastal boundary and was fairly constant from there to the coast. The wind speed generally increased along the entire transect from the uplands to the coast, with 1997 having reduced (by approximately 1 m s^{-1}) speeds compared to the other two years. The number of days with wind speeds greater than 5 m s^{-1} nearly doubled from the uplands (with an average of about 60 days) to the coast (with an average of about 110 days). Olsson et al. (2002) also provides an analysis of Kuparuk basin air temperature, humidity, and wind data.

The wind directions corresponding to these wind events also varied significantly from south to north (Fig. 5). In the southern portion of the domain (0–40 km in the ordinate of Fig. 2 and abscissa of Fig. 5), the wind directions were divided approximately equally among the east and west, with slightly more wind from the south. Between 40 and 140 km, winds predominantly came from the south and west. Between 140 km and the coast, winds were predominantly from the east or west. These easterly and westerly winds near the coast, and their influence on snow redistribution, have been documented by other researchers (e.g., Benson and Sturm 1993). Within the simulation domain, virtually no winds above 5 m s^{-1} came from the north. Field measurements of the orientation of snow-drift features, like dunes and sastrugi, confirm these basic wind direction patterns.

e. Data assimilation (to determine the precipitation)

To determine the total winter solid-precipitation distribution we adopted the following methodology. At the regional scale, such as that relevant to arctic Alaska winter precipitation mechanisms, local-scale erosion and deposition terms (d/dx, d/dy) in Eq. (1) largely average out and become negligible. In this case, the winter surface moisture balance becomes

$$\zeta^* = P^* + Q_v^*, \tag{3}$$

where ζ^* (m) is the end-of-winter snow-water-equivalent depth, P^* (m) is the winter-total snow-water-equivalent solid precipitation, and Q_v^*(m) is the winter-total blowing-snow snow-water-equivalent sublimation (a negative number from the perspective of the snow cover). We use SnowTran-3D to calculate Q_v^*, and our measured values to define ζ^*. Then we determine the precipitation values that satisfy Eq. (3). Thus, the resulting quality of P^* is dependent upon the accuracy of Q_v^* and ζ^*.

To determine the total winter precipitation, SnowTran-3D was run iteratively in ''data assimilation mode'' where we adjusted the model's precipitation input until the simulated end-of-winter snow-water-equivalent depths closely matched our measured south–north varying end-of-winter snow distributions. In this iterative procedure, our initial precipitation estimate was the measured south–north varying snow-water-equivalent distribution (Fig. 3), recognizing that this provided a lower bound on the required precipitation input. During subsequent iterations the model precipitation input at each time step was adjusted using the formula

$$P_{i+1}^*(y) = P_i^*(y) + [\zeta_{\text{obs}}^*(y) - \zeta_{\text{mod}}^*(y)], \tag{4}$$

where i is the iteration; ζ_{obs}^* is the observed end-of-winter snow-water-equivalent depth, defined by the polynomial-fitted curve given in Fig. 3 and Table 1; and ζ_{mod}^* is the modeled end-of-winter snow-water-equivalent depth. Here we have assumed that there was only south–north variation in P^* and ζ^* [and thus Q_v^*, through Eq. (3)].

The south–north varying modeled snow-water-equivalent depths [$\zeta_{\text{mod}}^*(y)$; 2301 values or positions] were computed by averaging all west–east model depth outputs (851 values) at each y position, effectively averaging out the local-scale variability resulting from erosion and deposition processes. During the model iterations, as P^* was adjusted, the Q_v^* distribution also changed. This is because the different P^* values modify the time at which the snow on the ground exceeded the vegetation snow-holding depth. This, in turn, modified the amount of available snow for wind transport. The solution was assumed to converge when the difference between $\zeta_{\text{obs}}^*(y)$ and $\zeta_{\text{mod}}^*(y)$ was less than 1% of $\zeta_{\text{obs}}^*(y)$ (about 0.1-cm snow-water-equivalent) for all values of y. This was achieved in five to eight iterations.

This data assimilation procedure for determining the precipitation has not been described previously, but we have used the same idea in a much less formal way to determine winter precipitation in other locations. These efforts include previous arctic Alaska snow-distribution simulations (Liston and Sturm 1998), alpine snow drift studies in Colorado and Wyoming (Greene et al. 1999; Hiemstra et al. 2002), hydrology studies in Norway (Bruland et al. 2002), and glacier mass-balance studies in Greenland (Hasholt et al. 2002). None of these studies explicitly produced P^* distributions, but all of them used an approach where by P^* was adjusted in SnowTran-3D until the modeled area-averaged snow depth equaled the observed value. These studies suggest that the methodology presented here is generally ap-

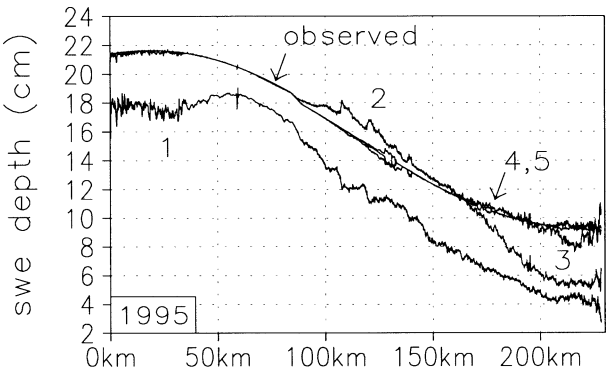

FIG. 6. Convergence of 1995 modeled snow-water-equivalent (swe) depth distribution toward the observed depth distribution. Shown are the south–north varying distributions for iterations 1, 2, 3, 4, and 5. The observed distribution from Fig. 3 is visually equivalent to iterations 4 and 5. The abscissa values correspond to the ordinate values in Fig. 2.

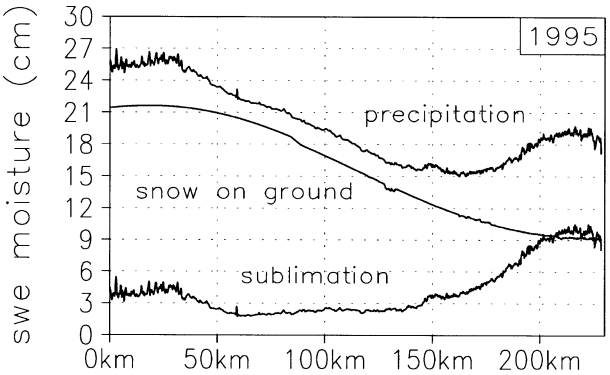

FIG. 7. Components of the 1995 moisture budget in snow-water-equivalent (swe) depth units. At each point along the curves, snow on ground = precipitation − sublimation. The abscissa values correspond to the ordinate values in Fig. 2.

plicable to other areas where wind redistribution of snow, and blowing-snow sublimation, are significant components of the winter landscape.

To meet the SnowTran-3D input requirement of a daily precipitation input that summed to equal the total winter precipitation quantities (P^*), solid precipitation was assumed to fall when the air temperature was below freezing and the relative humidity was greater than 80%. For each day that meets these criteria, the ratio of humidity in excess of 80% on that day, to the sum of humidity in excess of 80% for the entire winter, was computed. To produce a daily precipitation value, this daily ratio was multiplied by the total winter precipitation estimate. Liston and Sturm (1998) found SnowTran-3D snow distributions to be largely insensitive to the threshold humidity value that determines the timing and magnitude of the precipitation events.

3. Results

a. Model simulations

The convergence of the 1995 model solution [using Eq. (4)] to the observed snow-water-equivalent depth distribution (Fig. 3) is shown in Fig. 6. The convergence behavior was similar for 1996 and 1997 (not shown). The three components of the winter snow distribution for 1995 (Fig. 7) show a precipitation maximum in the uplands region, and a minimum in the coastal region that includes a small secondary precipitation maximum just south of the coast. Total 1995 winter blowing-snow sublimation was a maximum in the windy coastal regions, and a minimum in the uplands. The high coastal sublimation offset the coastal precipitation to produce snow depths that decreased monotonically from the uplands to the coast.

Figure 8a shows the simulated snow-depth distribution for 1995. Superimposed on the regional (south–north) snow-depth variation summarized in Fig. 7 are local-scale variations resulting from 100-m to few-kilometer topographic and vegetation variations. Figure 8a displays these local erosion and deposition variations in the form of alternating bands of differing snow depths. At the regional scale, the deepest snow was in the uplands, and the shallowest snow was in the coastal regions. The precipitation fraction that sublimated during 1995 is given in Fig. 8b. Coincident with the greatest sublimation amounts occurring in the coastal regions (Fig. 7), the fraction of precipitation that sublimated was a maximum (25%–55%) in the coastal region between the south–north positions 140 and 230 km, and a minimum (5%–25%) in the uplands between 0 and 140 km (Fig. 8b). Figures 7 and 8 suggest that an important contributing factor to the low coastal snow depths is the high coastal sublimation. In contrast, the sublimation over the uplands is relatively constant, and the precipitation generally increases as one moves south from the uplands–coastal boundary. Thus, precipitation is playing a key role in defining uplands snow distributions, while sublimation is playing a key role in defining the coastal distributions.

The 1996 simulated patterns of snow depth and sublimation were similar to those of 1995, while the magnitudes of these distributions were different (not shown). The precipitation fraction that sublimated was a maximum (25%–55%) in the coastal region between 140 and 230 km, and a minimum (15%–45%) in the uplands between the south–north positions 0 and 140 km. The overall character of the 1997 snow-depth and sublimation patterns (not shown) were similar to those of 1995 and 1996. The local-scale snow-distribution variability and the sublimation fraction were less than in 1995 and 1996 because of the generally lower wind speeds in 1997 (Fig. 4c). In 1997 the precipitation fraction that sublimated was a maximum (15%–45%) in the coastal region, and a minimum (5%–15%) in the uplands.

The 1995, 1996, and 1997 south–north varying sublimation and precipitation averages are given in Figs. 9

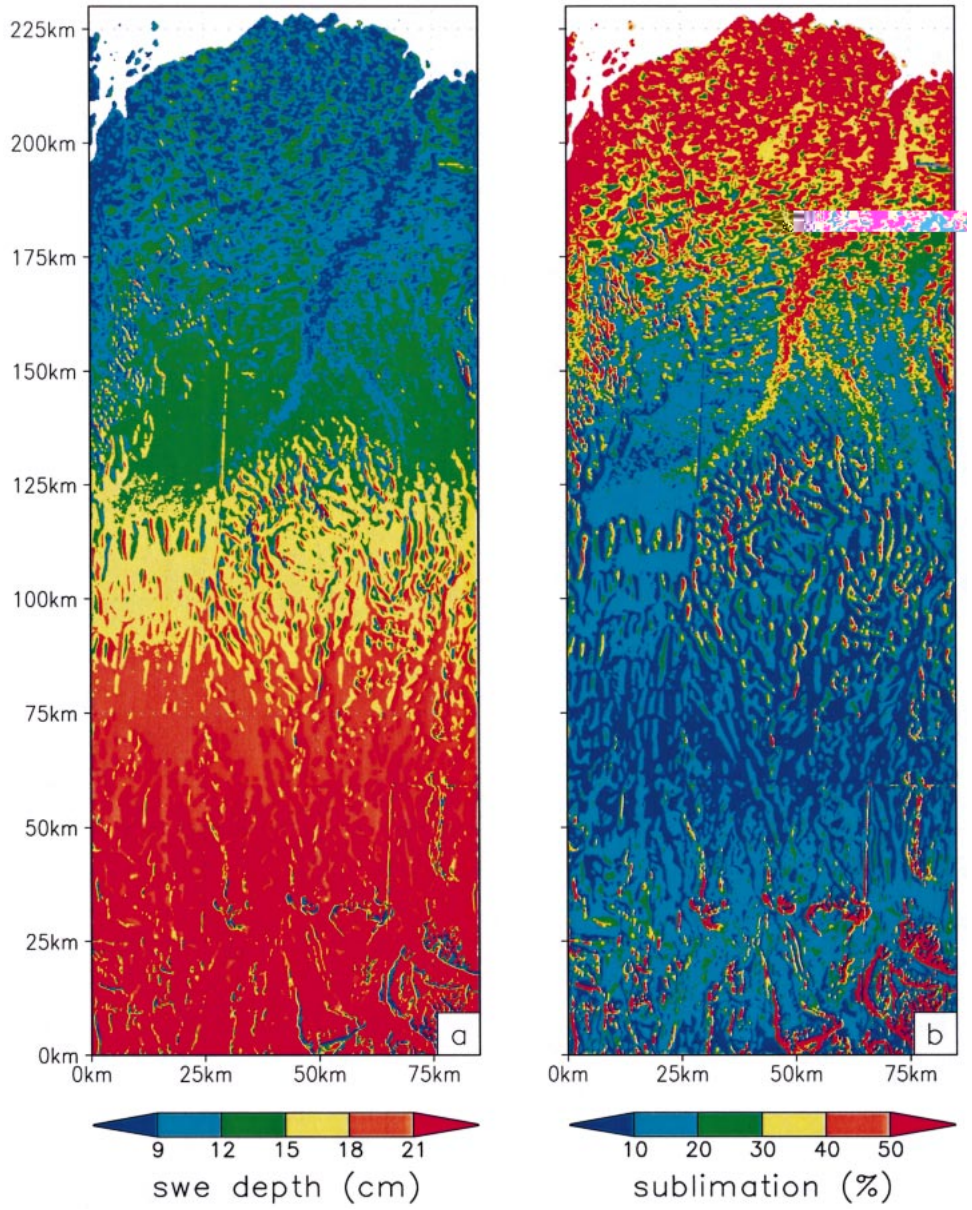

FIG. 8. Simulated 1995 Kuparuk basin (a) end-of-winter snow-water-equivalent (swe) depth distribution (i.e., snow on the ground), and (b) fraction of winter precipitation returned to the atmosphere by blowing-snow sublimation. The unrealistic linear features are the result of merging digital elevation datasets that have incompatible boundaries.

and 10, respectively. The uplands-, coastal-, and domain-averaged moisture quantities for each of the simulation years are given in Table 3. The fraction of precipitation that sublimated during blowing-snow events was quite uniform throughout the uplands (Fig. 9). The sublimation increased from the uplands–coastal boundary to the coast. During all three years the precipitation shows a well-defined maximum in the southern uplands, and a relatively constant minimum in the coastal regions (Fig. 10). During all three years there was a definite precipitation decrease from the southern uplands to the coastal regions.

In the northern half of the coastal region there is a significant 1995 precipitation maximum (Figs. 7 and 10). This is because of the greater number of days with wind speeds larger than 5 m s^{-1} (Fig. 4d) in 1995 (approximately 130) than in 1996 and 1997 (approximately 100); these wind events increase the snow transport, the blowing-snow sublimation, and the required precipitation contribution. As indicated in Fig. 2b, our snow

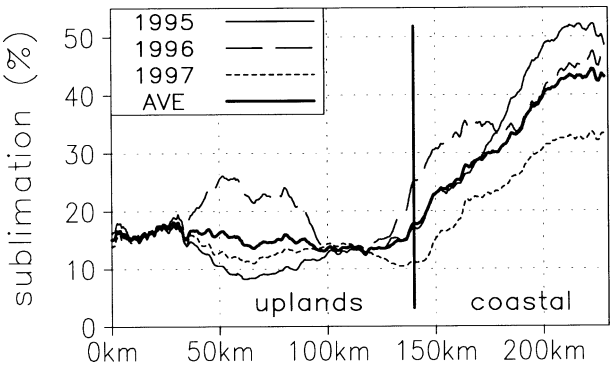

FIG. 9. South–north variation of the fraction of total winter precipitation returned to the atmosphere by blowing-snow sublimation, for each of the simulation years, and the 3-yr average. The abscissa values correspond to the ordinate values in Figs. 2 and 8. Also shown are the general coastal and uplands subregions. A 25-point line smoother was applied to the precipitation and sublimation curves to improve readability (compare with the unsmoothed curve in Fig. 7).

observations did not extend north of the 200-km position in the simulation domain, and the polynomial fit to the observations (Fig. 3) does not truly represent our knowledge of that area's snow distribution. Consequently, we also have less confidence in the simulated sublimation and precipitation values north of 200 km.

b. Comparison with precipitation observations

Within our Kuparuk simulation domain, there are three Wyoming-shielded precipitation gauges [see Yang et al. (2000) for a picture and a description]. The locations of these gauges correspond to the easternmost meteorological towers identified in Fig. 2b, at the northing positions 20 km (Imnavait Creek), 110 km (Sagwon), and 210 km (Prudhoe Bay). In an effort to assess

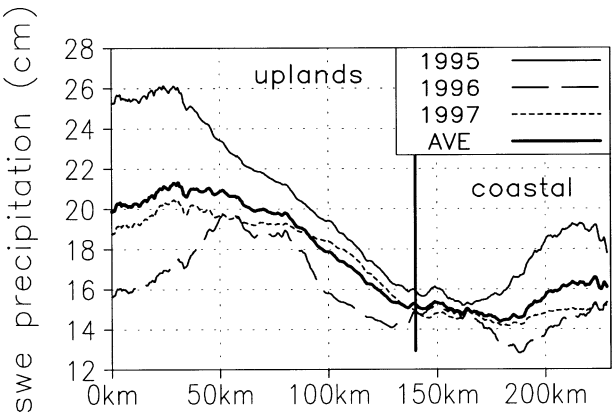

FIG. 10. South–north variation of the snow-water-equivalent precipitation, for each of the simulation years, and the 3-yr average. The abscissa values correspond to the ordinate values in Figs. 2 and 8. Also shown are the general coastal and uplands subregions. A 25-point line smoother was applied to the precipitation and sublimation curves to improve readability (compare with the unsmoothed curve in Fig. 7).

TABLE 3. Uplands-, coastal-, and domain-averaged, winter-total moisture balance quantities for each of the simulation years, in snow-water-equivalent depths (cm). Also shown is the precipitation fraction (%) that sublimated during blowing snow events.

	1995	1996	1997	3-yr average
	Uplands			
Snow on ground	18.8	13.6	16.1	16.2
Precipitation input	21.6	16.9	18.6	19.0
Sublimation loss	2.8	3.2	2.6	2.9
(% of precipitation)	(13)	(19)	(14)	(15)
	Coastal			
Snow on ground	10.5	9.0	11.0	10.2
Precipitation input	17.0	14.3	14.7	15.3
Sublimation loss	6.5	5.3	3.7	5.2
(% of precipitation)	(38)	(37)	(25)	(34)
	Total domain			
Snow on ground	15.6	11.8	14.1	13.8
Precipitation input	19.8	15.9	17.1	17.6
Sublimation loss	4.2	4.0	3.0	3.7
(% of precipitation)	(21)	(25)	(18)	(21)

the accuracy of the precipitation values calculated from the simulations described herein, we compared our values with the available Wyoming gauge precipitation data (Table 4).

For all of the uplands values in Table 4, the Wyoming gauge measurements are clearly unrealistic; in all cases we measured more snow on the ground than was caught by the gauge (the average gauge undercatch was 30%).

TABLE 4. Wyoming precipitation gauge data [snow-water equivalent (cm)]. Listed are the gauges within the Kuparuk simulation domain (see text for gauge locations), the data collected 1 Sep–30 Apr, for each of the simulation years. Also shown is the model-simulated precipitation [snow-water equivalent (cm)] at the gauge locations (from Fig. 10); the gauge undercatch (%), assuming the modeled precipitation is the true precipitation; and the observed snow depth [snow-water equivalent (cm)] at the gauge locations (from Fig. 3).

	1995	1996	1997
	Uplands		
Imnavait Creek			
Gauge precipitation	Missing data	13.0	13.5
Model precipitation	25.7	16.4	19.7
[Gauge undercatch (%)]	(−)	(21)	(31)
Snow on ground	21.6	13.8	16.6
Sagwon			
Gauge precipitation	12.4	10.4	11.9
Model precipitation	18.4	15.2	17.8
[Gauge undercatch (%)]	(33)	(32)	(33)
Snow on ground	16.4	13.2	15.4
	Coastal		
Prudhoe Bay			
Gauge precipitation	Missing data	16.8	14.5
Model precipitation	19.0	14.5	14.9
[Gauge undercatch (%)]	(−)	(−16)	(3)
Snow on ground	9.6	8.2	10.3

In a comparison of Imnavait Creek gauge snowfall records with observed Imnavait Creek snow-water-equivalent values for the years 1986–91, Yang et al. (2000) also found that gauge values were frequently less than the observed snow-water-equivalent depths. In addition, they found that, when the sublimation values calculated by Liston and Sturm (1998) were included, the mean Wyoming gauge undercatch was 32% for the 3 yr containing no missing data (1987, 1988, and 1990). Thus, the Liston and Sturm (1998) results are completely consistent with the uplands values calculated herein.

For the coastal station, in 1996 the Wyoming gauge measured 16% *more* precipitation than simulated by the model, suggesting that an even greater fraction of the coastal precipitation sublimated (51%) than was suggested by our simulations (43%). Yang and Ohata (2001) suggested that under very high wind speeds, precipitation gauges can catch horizontal blowing snow fluxes and thus overestimate the solid precipitation. In 1997, our simulations and the gauge precipitation values were quite similar, leading the fraction of precipitation that sublimated to be reduced from the modeled value of 31%, to 29%.

Clearly, for the uplands, even without considering our simulations, the Wyoming gauge data cannot be used without applying some kind of correction (there was more snow on the ground than was captured by the gauge). This correction must have some spatial and temporal dependence on environmental conditions (like wind speed) at each gauge. Yang et al. (2000) presented results from the WMO Solid Precipitation Measurement Intercomparison Project; gauge catch for the DFIR and the Wyoming gauge were compared under snowfall and blowing-snow conditions at four WMO intercomparison sites: Reynolds Creek, Idaho; Bismarck, North Dakota; Rabbit Ears Pass, Colorado; and Regina, Saskatchewan, Canada. Assuming that the DFIR collects the true precipitation [its undercatch, 5%–10% for high wind speeds, is much smaller than the other available gauges (Yang et al. 2000)], the average Wyoming gauge undercatches for snowfall and blowing-snow conditions were 6% and 55%, respectively.

Since the gauge corrections based on our model simulations (the undercatch listed in Table 4) generally fall within the 6% and 55% values listed by Yang et al. (2000), we believe our simulated values are reasonable. It is also clear that, although Wyoming gauge corrections are required to define the true precipitation, we do not know what those corrections should be. We anticipate that the gauge-correction factors will increase with increasing wind speed (e.g., Sturges 1986), and that, for conditions of turbulent-suspended snow transport during nonprecipitating events, the gauge catch may actually have to be reduced. Unfortunately, the conclusion is the same as that stated at the beginning of this paper: we are unable to accurately measure solid precipitation in windy, arctic conditions.

4. Discussion

Our methodology to determine the precipitation, sublimation, and snow-depth distributions requires that the following three components of the modeling system reasonably represent the natural system: 1) the snow-water-equivalent observations and the polynomial fit to them, 2) the atmospheric-forcing observations, and 3) the snow-transport model. While each of these components has its deficiencies (Liston and Sturm 1998; SL), they represent the current state of the science regarding snow-related arctic winter observational and modeling procedures and tools. Even though our methodology was only used to define south–north precipitation variations, it could be easily extended to include west–east variations if the west–east atmospheric-forcing and/or snow-depth variations were known.

Combining the three modeling system components has allowed us to estimate the solid-precipitation variability along an arctic Alaska transect from the Brooks Range to the Arctic Ocean in a physically realistic way. Our analyses show that the winter precipitation regimes are significantly different in the uplands and coastal regions, with a precipitation maximum in the uplands and a minimum on the coastal plain. Considerable interannual variability was found in the precipitation magnitudes, particularly in the uplands, although the general south–north distribution patterns were similar for all three years (Fig. 10). In the uplands, precipitation varied from 17-cm snow-water equivalent in 1996, to 22 cm in 1995. At the coast, precipitation varied from 14 to 17 cm, for 1996 and 1995, respectively. Averaged over the three simulation years, the uplands winter precipitation values were 24% greater than the coastal values.

In all three years the locations of the precipitation and snow-depth maximums and minimums coincided, while the sublimation had the opposite pattern (Figs. 3, 9, and 10). The sublimation spatial distribution can be largely explained by the south–north atmospheric-forcing variations (Fig. 4). Sublimation is greatest under conditions of high air temperature, low relative humidity, and high wind speeds. Thus, the temperature and humidity conditions were most favorable for sublimation in the uplands, but the wind speed was too low (Fig. 4). The increased wind speeds and frequency of wind events over 5 m s^{-1} in the coastal regions were enough to compensate for the relatively low temperatures and high humidities found there. In addition, the high humidities observed in the coastal regions may, in part, be the result of the high sublimation rates. One reason why these snow-related distributions are similar from year to year is that the factors that influence the snow characteristics and distributions are generally the same (Sturm et al. 1995). These factors are typically climate related and include such things as prevailing storm winds that are typically of a similar magnitude and come from a similar direction, similar precipitation–topography relationships, and similar air temperatures.

The 3-yr average precipitation fraction that sublimates was 15% in the uplands, and increased to 34% on the coastal plain (Table 3). In addition to the south–north sublimation variations, Fig. 8b shows that there were also considerable local (e.g., slope and aspect) sublimation variations, ranging from less than 5% to more than 50% of the precipitation. Pomeroy et al. (1998) also noted that blowing-snow sublimation fluxes can be a significant component of the winter moisture balance, and that these fluxes are not generally accounted for within current land–atmosphere interaction models. In a subdomain of the Kuparuk River basin, Liston and Sturm (1998) concluded that accounting for sublimation was required to produce the observed local-scale snow distributions.

The sublimation quantities computed as part of this study are comparable to those listed in previous prairie and arctic blowing-snow modeling studies (see the introduction). Since the sublimation submodels used in this study are similar to those used in these previous studies, we expect them to behave similarly, and we recognize the need to independently assess the quality of the sublimation outputs. Pomeroy and Essery (1999) presented such an analysis based on field observations of surface energy fluxes and found that the measured latent energy flux during blowing-snow events was reasonably simulated using the Prairie Blowing Snow Model (Pomeroy et al. 1993), a model that SnowTran-3D's sublimation formulation closely follows. What is really needed to validate the sublimation component of these models is a method to measure the true solid-precipitation amounts under conditions of nonzero wind speeds. This has long been recognized, but no acceptable solution has yet been presented. If the true precipitation and snow depth were known, then the sublimation could be calculated from the difference of these two variables.

The 1995, 1996, and 1997 simulated snow distributions (e.g., Fig. 8a) display two predominant spatial scales: a local scale and a regional scale. The local scale is dictated by the topographic and vegetation variability defined by the 100-m topography and vegetation datasets. At this scale the snow distributions were strongly dependent upon snow erosion on the windward sides and tops of ridges, and deposition on lee slopes and in valleys. At the regional scale, variability in the regional atmospheric forcing produced regional snow-distribution variations. Our modeling methodology, through Eqs. (3) and (4), has required that the simulations match the observed regional snow distributions, and has let the model simulate the local variations. These local snow-distribution variations arise from the model's simulation of wind speed variations in response to the variable topography (higher wind speeds on windward slopes, lower speeds on lee slopes, etc.). In our analyses we have not attempted to validate the local snow distributions but have assumed that they are reasonable based on the model's previous success in this area (Liston and Sturm 1998). The only significant difference between the model setup for the simulations discussed herein and those presented by Liston and Sturm (1998) is that we have used a 100-m instead of a 20-m grid increment. This has smoothed (or eliminated) the representation of small drift traps that exist within the domain due to higher-resolution vegetation and topographic variations.

5. Conclusions

A blowing-snow model (SnowTran-3D) that accounts for interactions between the atmosphere, vegetation, topography, and winter snow cover was used to describe the local and regional variations in snow distributions and atmospheric conditions over a 20 000-km^2 arctic Alaska domain. This region includes a variety of land cover types and topographic characteristics ranging from gently rolling ridges and valleys to flat plains. During the winter months, virtually all precipitation falls in solid form. The low-growing vegetation and high wind speeds that characterize the domain allow significant wind redistribution of snow throughout the winter. This means that snow depths can be quite variable and, under appropriate atmospheric conditions, some of the snow cover is returned to the atmosphere by blowing-snow sublimation.

Because reasonable (or even unreasonable) winter precipitation measurements do not generally exist in wind-blown arctic regions, and within our domain in particular, we have presented a methodology that uses snow-depth measurements and model-simulated blowing-snow sublimation to calculate the precipitation. This methodology consisted of solving the model equations in an iterative manner, while adjusting the precipitation inputs until the simulated snow-depth distributions matched our regional observations. In this way, we determined the precipitation distributions that produced a ''best fit'' with the regional snow-depth measurements. An attractive feature of this approach is that the model also quantifies the local and regional sublimation of wind-transported snow and simulates the local-scale snow-distribution characteristics, while reproducing the observed regional-scale snow distributions. By applying this methodology to a relatively large region, we have quantified regional precipitation distributions along a south–north transect across arctic Alaska. Because of the difficulty in making acurate winter precipitation measurements in such environments, our methodology has provided a plausible precipitation distribution where otherwise there would be none.

This research has highlighted important interrelationships and interactions that exist within the hydrologic and atmospheric components of the arctic climate system. Snow depths have been found to vary over a wide range of scales, and associated with these are important variations in winter precipitation and blowing-snow sublimation fluxes. The local and regional snow distri-

butions generated as part of this study can be used as part of hydrologic and ecologic studies interested in such things as the thermal regime of underlying soils (e.g., Taras et al. 2002), the depletion of snow-covered area during snowmelt, and snowmelt runoff. The sublimation distributions can be used to guide the development of sublimation parameterizations within regional and global land surface hydrology and atmospheric models. In addition, the computed precipitation fields can be used to validate solid-precipitation outputs from regional atmospheric models being applied to this area of the arctic, and the same methods can be used to produce precipitation fields in other arctic, prairie, and alpine regions where blowing snow is common.

Acknowledgments. The authors would like to thank Douglas L. Kane, Larry D. Hinzman, and their group at the Water and Environmental Research Center, University of Alaska, Fairbanks, for providing much of the meteorological data used to drive these model simulations; D. A. Walker, Institute of Arctic Biology, University of Alaska, Fairbanks, for providing the topographic and vegetation datasets; and Rick McClure, Natural Resources Conservation Service, Anchorage, for providing the Wyoming gauge precipitation data. We would also like to thank Laura C. Bowling, Richard Essery, Douglas L. Kane, Larry D. Hinzman, and Roger A. Pielke, Sr., for their insightful reviews of this paper. This work was supported by NOAA Grant NA67RJ0152, NASA Grant NAG5-4560, and by NSF Grants OPP-9415386 and OPP-9943467.

REFERENCES

Benson, C. S., 1982: Reassessment of winter precipitation on Alaska's Arctic Slope and measurements on the flux of wind blown snow. Rep. UAG R-288, Geophysical Institute, University of Alaska, 26 pp. [Available from Geophysical Institute, University of Alaska, P.O. Box 757320, Fairbanks, AK 99775-7320.]

——, and M. Sturm, 1993: Structure and wind transport of seasonal snow on the Arctic Slope of Alaska. *Ann. Glaciol.*, **18,** 261–267.

Bliss, L. C., and N. V. Matveyeva, 1992: Circumpolar arctic vegetation. *Arctic Ecosystems in a Changing Climate: An Ecophysiological Perspective,* F. S. Chapin III et al., Eds., Academic Press, 59–89.

Bruland, O., G. E. Liston, J. Vonk, K. Sand, and A. Killingtveit, 2002: Modelling the snow distribution at high arctic sites at Svalbard, Norway, and at a sub-arctic site in central Norway. *Nord. Hydrol.,* in press.

Essery, R., L. Li, and J. Pomeroy, 1999: A distributed model of blowing snow over complex terrain. *Hydrol. Processes,* **13,** 2423–2438.

Everett, K. R., D. L. Kane, and L. D. Hinzman, 1996: Surface water chemistry and hydrology of a small Arctic drainage basin. *Landscape Function: Implications for Ecosystem Response to Disturbance: A Case Study in Arctic Tundra,* J. F. Reynolds and J. D. Tenhunen, Eds., Ecologic Studies Series, Vol. 120, Springer-Verlag, 185–201.

Goodison, B. E., H. L. Ferguson, and G. A. McKay, 1981: Measurement and data analysis. *Handbook of Snow,* D. M. Gray and M. D. Male, Eds., Pergamon Press, 191–274.

Greene, E. M., G. E. Liston, and R. A. Pielke Sr., 1999: Simulation of above treeline snowdrift formation using a numerical snow-transport model. *Cold Reg. Sci. Technol.,* **30,** 135–144.

Hasholt, B., G. E. Liston, and N. T. Knudsen, 2002: Snow distribution modelling in the Ammassalik Region, south east Greenland. *Nord. Hydrol.,* in press.

Hiemstra, C. A., G. E. Liston, and W. A. Reiners, 2002: Snow redistribution by wind and interactions with vegetation at upper treeline in the Medicine Bow Mountains, Wyoming, U.S.A. *Arct. Antarct. Alp. Res.,* **34,** 262–273.

Hinzman, L. D., D. L. Kane, C. S. Benson, and K. R. Everett, 1996: Energy balance and hydrological processes in an Arctic watershed. *Landscape Function: Implications for Ecosystem Response to Disturbance. A Case Study in Arctic Tundra,* J. F. Reynolds and J. D. Tenhunen, Eds., Ecologic Studies Series, Vol. 120, Springer-Verlag, 131–154.

——, D. J. Goering, and D. L. Kane, 1998: A distributed thermal model for calculating soil temperature profiles and depth of thaw in permafrost regions. *J. Geophys. Res.,* **103** (D22), 28 975–28 991.

Jeffries, M. O., K. Morris, and G. E. Liston, 1996: A method to determine lake depth and water availability on the North Slope of Alaska with spaceborne imaging radar and numerical ice growth modelling. *Arctic,* **49,** 367–374.

Kane, D. L., L. D. Hinzman, C. S. Benson, and G. E. Liston, 1991: Snow hydrology of a headwater Arctic basin. 1. Physical measurements and process studies. *Water Resour. Res.,* **27,** 199–1109.

König, M., and M. Sturm, 1998: Mapping snow distribution in the Alaskan Arctic using air photos and topographic relationships. *Water Resour. Res.,* **34,** 3471–3483.

Larson, L. W., and E. L. Peck, 1974: Accuracy of precipitation measurements for hydrologic modeling. *Water Resour. Res.,* **10,** 857–863.

Liston, G. E., 1995: Local advection of momentum, heat, and moisture during the melt of patchy snow covers. *J. Appl. Meteor.,* **34,** 1705–1715.

——, 1999: Interrelationships among snow distribution, snowmelt, and snow cover depletion: Implications for atmospheric, hydrologic, and ecologic modeling. *J. Appl. Meteor.,* **38,** 1474–1487.

——, and D. K. Hall, 1995: An energy balance model of lake ice evolution. *J. Glaciol.,* **41,** 373–382.

——, and M. Sturm, 1998: A snow-transport model for complex terrain. *J. Glaciol.,* **44,** 498–516.

——, J.-G. Winther, O. Bruland, H. Elvehøy, K. Sand, and L. Karlöf, 2000: Snow and blue-ice distribution patterns on the coastal Antarctic ice sheet. *Antarct. Sci.,* **12,** 69–79.

——, J. P. McFadden, M. Sturm, and R. A. Pielke Sr., 2002: Modeled changes in arctic tundra snow, energy, and moisture fluxes due to increased shrubs. *Global Change Biol.,* **8,** 17–32.

Marsh, P., 1999: Snowcover formation and melt: Recent advances and future prospects. *Hydrol. Processes,* **13,** 2117–2134.

McFadden, J. P., G. E. Liston, M. Sturm, R. A. Pielke Sr., and F. S. Chapin III, 2001: Interactions of shrubs and snow in arctic tundra: Measurements and models. *Soil, Vegetation, Atmosphere Transfer Schemes and Large-Scale Hydrological Models,* A. J. Polman et al., Eds., IAHS, Publ. 270, 317–325.

McNamara, J. P., D. L. Kane, and L. D. Hinzman, 1997: Hydrograph separations in an Arctic watershed using mixing model and graphical techniques. *Water Resour. Res.,* **33,** 1707–1719.

——, ——, and ——, 1998: An analysis of streamflow hydrology in the Kuparuk River basin, arctic Alaska: A nested watershed approach. *J. Hydrol.,* **206,** 39–57.

——, ——, and ——, 1999: An analysis of an arctic channel network using a digital elevation model. *Geomorphology,* **29,** 339–353.

Nelson, F. E., K. M. Hinkel, N. I. Shiklomanov, G. R. Mueller, L. L. Miller, and D. K. Walker, 1998: Active-layer thickness in north central Alaska: Systematic sampling, scale, and spatial autocorrelation. *J. Geophys. Res.,* **103** (D22), 28 963–28 973.

Neumann, N., and P. Marsh, 1998: Local advection of sensible heat

in the snowmelt landscape of Arctic tundra. *Hydrol. Processes,* **12,** 1547–1560.

Olsson, P. Q., L. D. Hinzman, M. Sturm, G. E. Liston, and D. L. Kane, 2002: Surface climate and snow-weather relationships of the Kuparuk basin on Alaska's Arctic Slope. ERDC/CRREL Tech. Rep. TR-02-10, Cold Regions Research and Engineering Laboratory, Engineer Research and Development Center, U.S. Army Corps of Engineers, 50 pp.

Pomeroy, J. W., and D. M. Gray, 1995: Snowcover accumulation, relocation and management. National Hydrology Research Institute Science Rep. 7, Hydrological Sciences Division, NHRI Division of Hydrology, University of Saskatchewan, Saskatoon, SK, Canada, 144 pp.

——, and R. L. H. Essery, 1999: Turbulent fluxes during blowing snow: Field test of model sublimation predictions. *Hydrol. Processes,* **13,** 2963–2975.

——, D. M. Gray, and P. G. Landine, 1993: The Prairie Blowing Snow Model: Characteristics, validation, operation. *J. Hydrol.*, **144,** 165–192.

——, P. Marsh, and D. M. Gray, 1997: Application of a distributed blowing snow model to the Arctic. *Hydrol. Processes,* **11,** 1451–1464.

——, D. M. Gray, K. R. Shook, B. Toth, R. L. H. Essery, A. Pietroniro, and N. Hedstrom, 1998: An evaluation of snow accumulation and ablation processes for land surface modelling. *Hydrol. Processes,* **12,** 2339–2367.

Prasad, R., D. G. Tarboton, G. E. Liston, C. H. Luce, and M. S. Seyfried, 2001: Testing a blowing snow model against distributed snow measurements at Upper Sheep Creek. *Water Resour. Res.,* **37,** 1341–1357.

Schmidt, R. A., 1972: Sublimation of wind-transported snow—A model. Research Paper RM-90, Rocky Mountain Forest and Range Experiment Station, USDA Forest Service, Fort Collins, CO, 24 pp.

——, 1982: Vertical profiles of wind speed, snow concentration, and humidity in blowing snow. *Bound.-Layer Meteor.,* **23,** 223–246.

——, 1991: Sublimation of snow intercepted by an artificial conifer. *Agric. For. Meteor.,* **54,** 1–27.

Sturges, D. L., 1986: Precipitation measured by dual gages, Wyoming shielded gages and in a forest opening. *Proceedings of the Cold Regions Hydrology Symposium,* D. L. Kane Ed., Amer. Water Resour. Assoc., 387–396.

Sturm, M., J. Holmgren, and G. E. Liston, 1995: A seasonal snow cover classification system for local to global applications. *J. Climate,* **8,** 1261–1283.

——, G. E. Liston, C. S. Benson, and J. Holmgren, 2001a: Characteristics and growth of a snowdrift in arctic Alaska. *Arct. Antarct. Alp. Res.,* **33,** 319–329.

——, J. P. McFadden, G. E. Liston, F. S. Chapin III, C. H. Racine, and J. Holmgren, 2001b: Snow–shrub interactions in Arctic tundra: A hypothesis with climate implications. *J. Climate,* **14,** 336–344.

Tabler, R. D., 1975: Estimating the transport and evaporation of blowing snow. *Proc. Symp. on Snow Management on the Great Plains,* Bismarck, ND, Great Plains Agricultural Council Publ. 73, 85–104.

Taras, B., M. Sturm, and G. E. Liston, 2002: Snow–ground interface temperatures in the Kuparuk River basin, arctic Alaska: Measurements and model. *J. Hydrometeor.,* **3,** 377–394.

Yang, D., and T. Ohata, 2001: A bias-corrected Siberian regional precipitation climatology. *J. Hydrometeor.,* **2,** 122–139.

——, B. E. Goodison, J. R. Metcalfe, V. S. Golubev, R. Bates, T. Pangburn, and C. L. Hanson, 1998: Accuracy of NWS 8 standard nonrecording precipitation gauge: Results and application of WMO intercomparison. *J. Atmos. Oceanic Technol.,* **15,** 54–68.

——, and Coauthors, 2000: An evaluation of the Wyoming gauge system for snowfall measurement. *Water Resour. Res.,* **36,** 2665–2677.